Observation of attractive and repulsive polarons in a Bose-Einstein condensate

N. B. Jørgensen,[1] L. Wacker,[1] K. T. Skalmstang,[1] M. M. Parish,[2] J. Levinsen,[2] R. S. Christensen,[1] G. M. Bruun,[1] and J. J. Arlt[1]

[1]*Institut for Fysik og Astronomi, Aarhus Universitet, 8000 Aarhus C, Denmark.*
[2]*School of Physics & Astronomy, Monash University, Victoria 3800, Australia.*
(Dated: April 28, 2016)

The behavior of a mobile impurity particle interacting with a quantum-mechanical medium is of fundamental importance in physics. Due to the great flexibility of atomic gases, our understanding of the impurity problem has improved dramatically since it was realized experimentally in a particularly pure form using degenerate Fermi gases [1–3]. However, there has not been such a realization of the impurity problem in a bosonic reservoir so far. Here, we use radio frequency spectroscopy of ultracold bosonic ^{39}K atoms to experimentally demonstrate the existence of a well-defined quasiparticle state for an impurity interacting with a Bose-Einstein condensate (BEC). We measure the energy of the impurity both for attractive and repulsive interactions with the BEC, and find excellent agreement with theories that incorporate three-body correlations, both in the weak-coupling limits and across unitarity. Our results show that the spectral response consists of a well-defined quasiparticle peak at weak coupling and a continuum of excited many-body states. For increasing interaction strength, the spectrum is strongly broadened and becomes dominated by the many-body continuum, but no significant effects of three-body decay are observed. Our results open up intriguing prospects for studying mobile impurities in a bosonic environment, as well as strongly interacting Bose systems in general.

The scenario of an impurity interacting with its environment has provided deep insight into quantum many-body systems. Since Landau and Pekar first proposed that the coupling between electrons and lattice phonons leads to the existence of quasiparticles termed polarons [4], this idea has systematically been developed [5]. The concept of the polaron is now central to our understanding of a wide range of materials including technologically important semiconductors [6]. The "dressing" of a particle by a bosonic reservoir plays an important role in many other systems, such as ^{3}He–^{4}He mixtures [7] and high temperature superconductors [8]. Indeed, even the elementary particles of the Standard Model acquire their mass by coupling to the bosonic Higgs particle. It is therefore highly desirable to understand the properties of an impurity particle immersed in a bosonic reservoir. Several specific cases have been investigated using atomic Bose gases: impurities interacting with an uncondensed bosonic medium [9], charged or fixed impurities in a BEC [10–13], and impurities confined to a lattice [14]. However, there has not yet been a realization of the canonical mobile impurity in a BEC – the Bose polaron – despite intense theoretical investigation [15–23].

We investigate the Bose polaron using a harmonically trapped BEC of ^{39}K atoms initially prepared in the $|1\rangle \equiv$
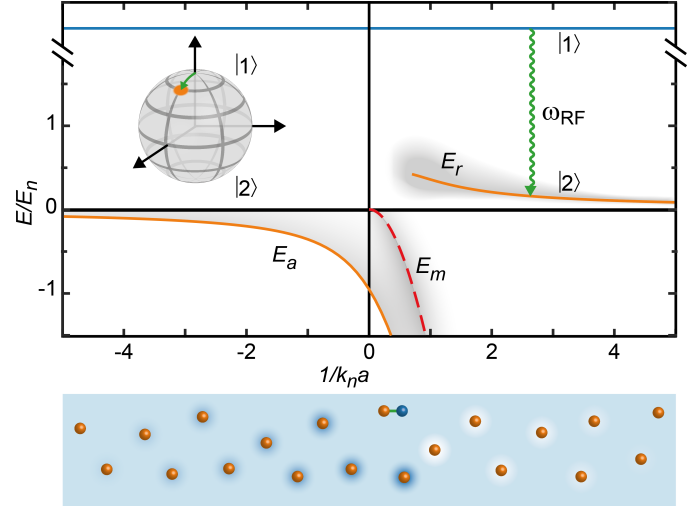

FIG. 1. **Sketch of the spectroscopic method and the impurity energy spectrum.** A radio frequency pulse transfers atoms from the $|1\rangle$ to the $|2\rangle$ state. Only a small fraction is transferred, corresponding to a rotation by a small angle on the Bloch sphere (inset) in a non-interacting system. The solid lines show the energies of the zero-momentum attractive (E_a) and repulsive (E_r) polaron states in a uniform BEC as a function of the interaction parameter $1/k_n a$ (see text). The dashed line shows the molecular binding energy E_m (Methods) on the repulsive side of the Feshbach resonance, and the gray shading denotes a continuum of many-body states. The bottom cartoon shows impurity atoms (orange) in a BEC (blue); the intensity of the background color indicates the change in the BEC density due to the presence of impurity atoms.

$|F = 1, m_F = -1\rangle$ state (Methods). The BEC has average density $n_0 = 2.3 \times 10^{14}$cm^{-3}, which we parameterize by the wavenumber $k_n = (6\pi^2 n_0)^{1/3}$. The $|1\rangle$ atoms are weakly interacting with scattering length a_B such that $k_n a_B \approx 0.01$. To introduce impurities, we apply a radio frequency (RF) pulse of $100\,\mu$s duration, which transfers a small fraction of atoms into the $|2\rangle \equiv |F = 1, m_F = 0\rangle$ state (Figure 1). This scheme is advantageous since it ensures a perfect spatial overlap of impurities with the BEC. Furthermore, it is unique to a bosonic system since interaction effects in a Fermi gas subjected to a coherent RF pulse would be suppressed due to the Pauli principle [24]. We transfer less than 10% of the atoms into the $|2\rangle$ state, such that they can be regarded as isolated mobile impurities (Supplementary Information).

The transition frequency $\omega_{\rm RF}$ between the two hyperfine states is changed from its unperturbed value ω_0 due to the impurity-BEC interactions, as shown schematically in Fig. 1. This interaction is characterized by the *s*-wave scattering length a between $|1\rangle$ and $|2\rangle$ atoms, which is highly tunable
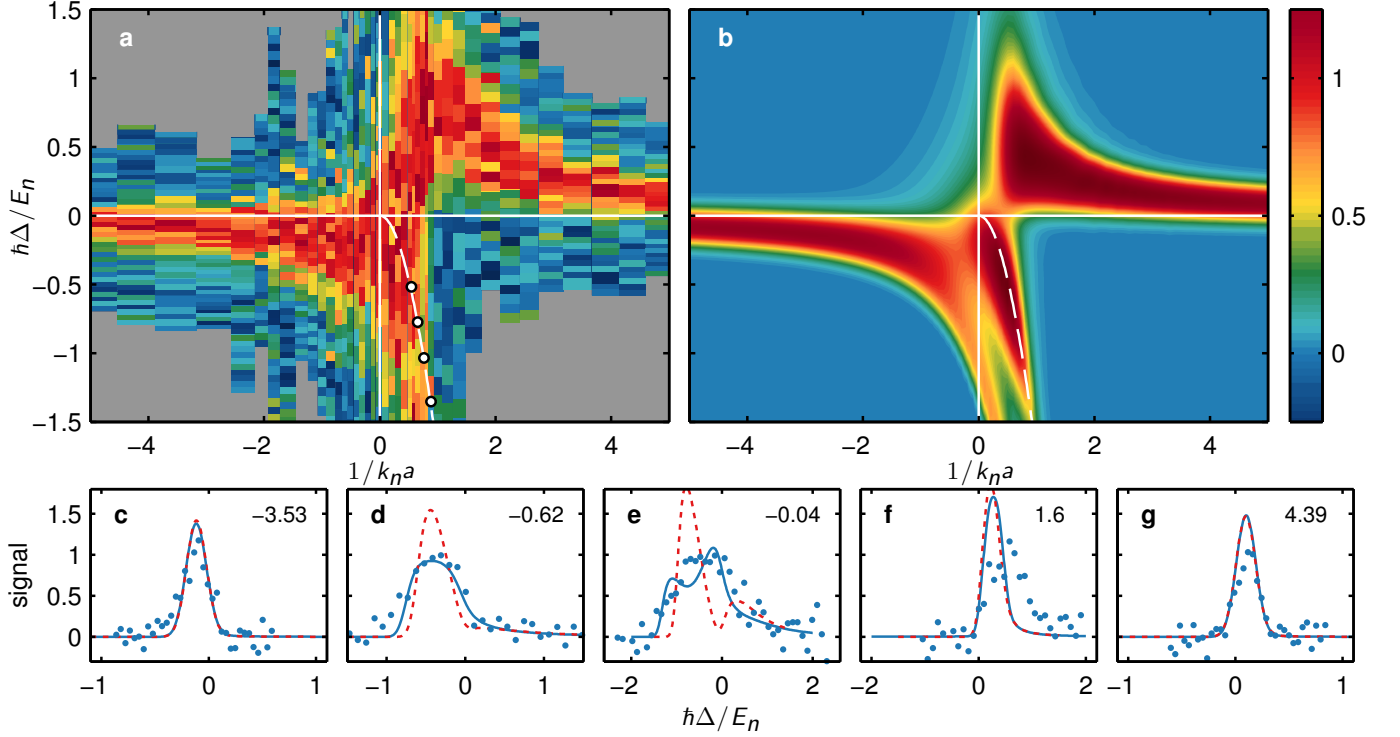
FIG. 2. **Spectral response of the impurity in the BEC.** The false color plots show the experimentally measured spectroscopic signal (a) and the calculated spectrum (b), for different values of detuning Δ and the interaction parameter $1/k_n a$. The theoretical calculation includes a spatial average over the trapped BEC and a convolution with the Fourier width of the RF pulse (Supplementary Information). The experimental spectrum is recorded such that its peak amplitude is constant for all values of $1/k_n a$. Accordingly, the theoretical spectrum is normalized such that its frequency integrated weight is the same as the experimental spectrum. In addition, the independently measured molecular binding energy (white dots) and a fit to it (dashed line) are shown. Negative values of the experimental signal are due to shot-to-shot atom number fluctuations (Methods). Panels **(c)-(g)** show the signal as a function of Δ for various values of $1/k_n a$ (see panel). The solid lines show the calculated signal using the truncated basis method including three-body correlations; this is in excellent agreement with the experiment, except for $1/k_n a = 1.6$ where the agreement is qualitative. The dashed lines, obtained excluding three-body correlations, only agree with the experiment for weak interactions.

using a Feshbach resonance located at $113.8\,\mathrm{G}$ [25]. Following the RF pulse and a variable hold time, the trap is switched off and the atom cloud is allowed to expand for 23 ms. Within the first part of this sequence the atomic cloud suffers losses due to three-body collisions between the $|1\rangle$ and $|2\rangle$ atoms at high density. For a given scattering length a, we measure the resulting atom number in the $|1\rangle$ state as a function of detuning $\Delta = \omega_0 - \omega_{\mathrm{RF}}$ and thus perform spectroscopy on the $|1\rangle \rightarrow |2\rangle$ transition (Methods). The detuning is parameterized by the energy scale of the system $E_n = \hbar^2 k_n^2/2m$ where m is the mass of ^{39}K.

Figure 1 illustrates the behavior of the zero-momentum impurity in a uniform BEC of density n_0. For weak interactions, $1/k_n a \ll -1$ and $1/k_n a \gg 1$, the impurity forms well-defined quasiparticle states termed attractive and repulsive polaron, respectively. These have mean-field energy $4\pi\hbar^2 n_0 a/m$ plus medium corrections which have recently been determined up to order a^3 [22]. On the attractive side of the Feshbach resonance, the zero-momentum attractive polaron is the ground state. In the absence of Efimov physics [26], the attractive polaron state exhibits an avoided crossing with the molecular

state beyond unitarity [18, 23]. Above the ground state there is a continuum of many-body states, which in the weakly interacting limit is formed by polarons and Bogoliubov excitations with zero total momentum (Supplementary Information). On the repulsive side $1/k_n a > 0$, the repulsive polaron becomes increasingly damped when approaching the Feshbach resonance, since it can decay into lower lying states and is inherently metastable.

Figure 2 compares the measured spectroscopic signal with that expected for a zero-momentum impurity within linear response (Methods). The theoretical spectrum reproduces the observed signal strikingly well, both for attractive and repulsive interactions. In particular, both experiment and theory show a clear shift in the observed spectral weight due to the interaction between the impurity and the BEC. The calculation of the spectrum involves a restricted Hilbert space of impurity wavefunctions such that at most two Bogoliubov excitations of the BEC are included (Supplementary Information). Crucially, this truncated basis method (TBM) [27] allows us to include three-body correlations in the spectral function *nonperturbatively*, and thus model the continuum of excited po-
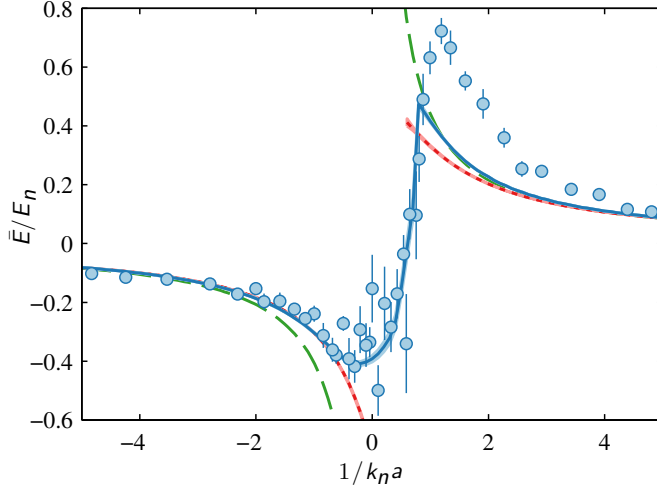
FIG. 3. **Average energy of the impurity state.** The average energy $\bar{E}$ of the impurity spectrum is shown as a function of the interaction parameter. The energy was obtained from Gaussian fits to the spectroscopic signal (blue dots) and to the full TBM spectrum (blue line). For comparison, we display the results for a TBM spectrum without three-body correlations (red line) and from perturbation theory (dashed line) (Supplementary Information).

laron states. Figure 2(c)-(g) shows cuts through the spectrum at fixed $1/k_n a$, demonstrating that the inclusion of three-body correlations in the spectrum is essential for an accurate description of the strongly interacting unitary regime.

In contrast to the Fermi polaron [1, 2], there is no sharp transition to a molecular state and the attractive polaron quasiparticle remains the ground state of the system for all interaction strengths. However, the spectral weight of the polaron is increasingly transferred to the continuum of higher-lying states as the strongly interacting unitary regime is approached from the attractive side of the Feshbach resonance. This feature is clearly apparent in both the observed and the calculated spectral response in Fig. 2. For $1/k_n a > 0$, the structure of this continuum is determined by the molecular branch, and in the theoretical spectrum we see a clear suppression of spectral weight between the ground-state quasiparticle and the continuum. This is not apparent in the experimental spectrum, potentially due to atom number fluctuations or correlation effects not included in the theory. Significantly, the theory correctly captures the abrupt decrease in the observed signal at negative detuning for $1/k_n a \gtrsim 1$, where the molecule becomes deeply bound compared to E_n. The detailed comparison of spectroscopic signals in Fig. 2 (c)-(e) further highlights the excellent agreement between theory and experiment for the attractive branch.

To further quantify the results, Fig. 3 compares the average impurity energy obtained from theory and experiment. For the attractive polaron, the experimental data agrees well with the results of the TBM. This holds even in the strongly interacting unitary regime up to and including the abrupt shift of spectral weight to positive detuning at $1/k_n a \simeq 1$. In the case of the repulsive polaron, the agreement is good for weak
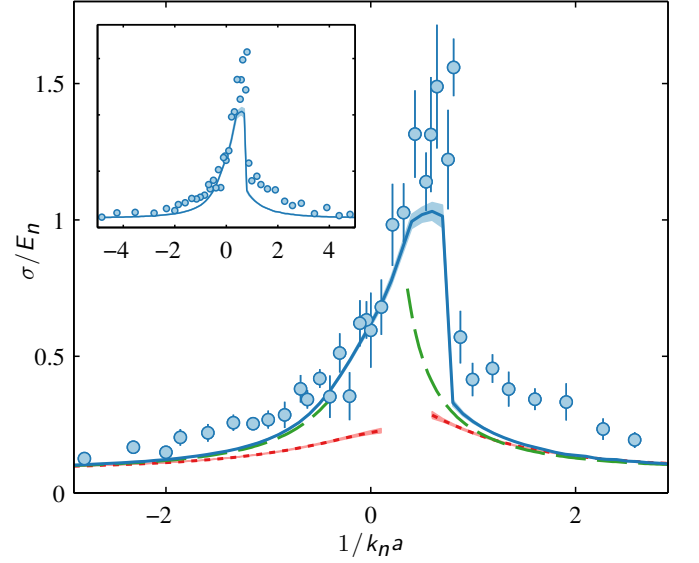

FIG. 4. **Width of the spectrum.** The width σ of the impurity spectrum is shown as a function of the interaction parameter. The widths were obtained from Gaussian fits to the spectroscopic signal (blue dots), the full TBM spectrum (blue line), and the TBM without three-body correlations (red line). The green dashed line was obtained from a spatial average and Fourier width convolution of the result from perturbation theory excluding the many-body continuum (Supplementary Information). The inset shows the width for the entire experimental data set compared with the full TBM spectrum.

interaction, whereas there is only qualitative agreement for $1 \lesssim 1/k_n a \lesssim 3$. This suggests that there are important aspects of the experiment that have not been included in the theory, such as effects of temperature, three-body recombination to deeply bound states, and multiple excitations of the BEC. The last effect is likely to play a role for strong interactions near $1/k_n a \simeq 1$, since the repulsive branch in this regime involves a broad continuum of many-body states, which is challenging to model. For comparison, Fig. 3 also includes the result of the TBM without three-body correlations, highlighting the necessity of their inclusion.

Importantly, the perturbative result for the polaron energy [22] accurately reproduces the observed energy shift in Fig. 3 for weak attractive and repulsive interactions. From this we conclude that the experimental data confirms the existence of a well-defined Bose polaron quasiparticle in this regime.

The width of the spectral response also agrees well with theory for interaction parameters $1/k_n a \lesssim 1$ and $1/k_n a \gtrsim 3$, as shown in Fig. 4. For weak interactions, the spectral broadening arises mainly from the Fourier width of the RF pulse and the density inhomogeneity of the trapped BEC. This is illustrated by the fact that the perturbative result assuming a perfect undamped polaron reproduces the observed width in this regime (Supplementary Information). However, near unitarity where the system is strongly correlated, the spectral weight of the polaron is small, and the many-body continuum of states accounts for the significant broadening of the spectrum. Im-

portantly, this effect is captured by the TBM when three-body correlations are included. For the strongly interacting repulsive branch, there is again only qualitative agreement between theory and experiment for the reasons outlined above.

Since strongly interacting Bose systems are expected to suffer from rapid three-body recombination, it is striking how well the experimental observations are described by theories that neglect such losses. The observed width of the spectrum is explained by the trap inhomogeneity, Fourier broadening, and the many-body continuum. We note that the impurity decay rate, which is proportional do $n_0^2 a^4$ when $n_0|a|^3 \ll 1$, is ultimately limited by the average interparticle spacing in the unitary regime. In this case the energy shift and decay rate both scale as $n_0^{2/3}$. Our results thus imply that the ratio of the decay rate to the energy shift at unitarity remains small, a finding which is consistent with the recent experiment on the unitary Bose gas [28].

Our observation of a well-defined Bose polaron opens up the exciting opportunity to study quantum impurities in a bosonic environment systematically and in regimes never realized before. For instance, an intriguing question is how the polaron changes when the BEC melts. The effects of such a phase transition of the environment on an impurity particle has never been investigated before. There is also the prospect of observing stable Efimov trimers in a BEC for the first time. We do not expect to observe a well-defined Efimov state in our present experiment, since the size of the smallest Efimov trimer is estimated to be 100 times larger than the interparticle spacing [23]. However, the Efimovian regime can be accessed by lowering the density or by using light impurities.

METHODS

Sample preparation. The experimental apparatus used to produce ^{39}K BECs was described in detail in [29]. Briefly, a dual-species magneto-optical trap captures ^{87}Rb and ^{39}K atoms and subsequently evaporative cooling is performed in a magnetic trap. All ^{87}Rb atoms are evaporated leading to sympathetic cooling of ^{39}K and the remaining ^{39}K atoms are loaded into an optical dipole trap consisting of two crossed beams at a wavelength of 1064nm. Finally ^{39}K is prepared in the $|1\rangle$ state, and the sample is evaporatively cooled further by lowering the dipole trap power. During this evaporation, a Feshbach resonance at 33.6 G is addressed to assure efficient rethermalization. When a sufficiently low temperature is reached, the magnetic field is ramped to the desired field in the vicinity of the Feshbach resonance at 113.8 G. During this process, the power of the dipole trap is raised to increase the density of the BEC, which results in trap frequencies of $\nu_x = 158$ Hz, $\nu_y = 167$ Hz and $\nu_z = 228$ Hz. Prior to the creation of polarons, the ^{39}K BEC consists of $\approx 2 \times 10^4$ atoms at a temperature of 160 nK corresponding to $T/T_c \approx 0.6$ where T_c is the critical temperature of Bose-Einstein condensation.

Inter-state Feshbach resonance. Our measurements of the polaron are carried out by employing an inter-state Feshbach resonance at 113.8 G [25], which allows for tuning of the interaction between atoms in the $|1\rangle$ and $|2\rangle$ states. The

Feshbach resonance was characterized by performing spectroscopy on the molecule state with binding energy $\frac{\hbar^2}{4mR^{*2}} \times (\sqrt{1 + 4R^*/a} - 1)^2$ and by determining the zero-crossing of the interaction in a rethermalization measurement of the components $|1\rangle$ and $|2\rangle$. This allowed us to parametrize the scattering length according to $a = a_{\text{bg}}(1 - \Delta B/(B - B_0))$ with $B_0 = 113.83$ G, $\Delta B = -15.93$ G and $a_{\text{bg}} = -45.24a_0$ where a_0 is the Bohr radius. Based on [25], the range parameter $R^* = \hbar^2/m a_{\text{bg}} \delta \mu \Delta B$ is estimated to be $60 a_0$.

Measurement procedure. To form the polaron, we use a square RF pulse of 100 μs duration. The pulse length and experimental magnetic field precision result in a spectral FWHM of $0.15 E_n$. A small fraction of $|1\rangle$ atoms is thus transferred into the $|2\rangle$ state and the sample is kept in the trap for a variable hold time before being released. After 5 ms of expansion, a strong magnetic field gradient is applied which separates the $|1\rangle$ and $|2\rangle$ components before absorption imaging after a total expansion time of 23 ms .

Three-body recombination processes involving two $|1\rangle$ and one $|2\rangle$ atom lead to a loss of atoms from the sample. Due to the large atom number imbalance we typically do not detect $|2\rangle$ atoms and only a decrease in $|1\rangle$ BEC atoms is observed. Since we found that the relative number of lost atoms did not depend on the hold time, this was set to zero for the majority of our measurements. Hence, the three-body recombination loss process occurs during the initial expansion time while the sample is sufficiently dense.

Due to the three-body recombination process, the number of lost atoms is three times larger than the number of atoms transferred to the polaron state. To obtain a maximal polaron fraction of 10% for each interaction strength, the power of the RF pulse was hence chosen to provide a maximum loss of approximately 30%.

Data evaluation. The spectroscopic signal is provided by the loss of $|1\rangle$ atoms from the BEC after the RF pulse. To convert this loss into the signal shown in Fig. 2 (a), the remaining number of atoms in the $|1\rangle$ state as a function of Δ was fitted with a Gaussian function for each value of $1/k_n a$. Based on the background BEC atom number and the peak atom number loss obtained from the fit, the normalized relative loss corresponding to the spectroscopic signal is obtained. Shot-to-shot atom number fluctuations can thus lead to negative values of the spectroscopic signal.

Conventionally, the spectral weight of the polaron spectrum is normalized to 2π. However, the integrated area of the experimentally obtained signal varies throughout the measured range of interaction strengths. To allow for a comparison, the theoretical spectrum in Fig. 2 (b) was normalized at each value of $1/k_n a$ to match the integrated area of the experimental signal in Fig. 2 (a) (Supplementary Information).

The spectra in Fig. 2 allow for an excellent visual comparison of the experimental signal and the calculated spectrum. However, further analysis is required for the quantitative comparison in Fig. 3 and 4. Since the calculated lineshape is unique for each value of $1/k_n a$, the theoretical result does not provide a general fit function that can be applied to the experimental data. Hence Gaussian fits to the spectroscopic signal and the calculated spectrum at fixed $1/k_n a$ are used to quan-

titatively compare experiment and theory. They allow for the comparison of the average energy and spectral width shown in Fig. 3 and 4 respectively. In the range $0 \lesssim 1/k_n a \lesssim 0.5$ this analysis technique fails for the TBM without three-body correlations and has been excluded from the figures.

Theory of the RF probe and the spectral response. The RF probe, which transfers atoms in spin state $|1\rangle$ into spin state $|2\rangle$ is described by the operator $H_{\mathrm{rf}} = \Omega e^{-i\omega t} \sum_{\mathbf{k}} a_{\mathbf{k}2}^{\dagger} a_{\mathbf{k}1} +$ h.c. Here, Ω is the Rabi frequency determined by the coupling between the spin states induced by the electromagnetic field, and ω is the field frequency. Within linear response, the resulting rate of transfer into state $|2\rangle$ is given by $\dot{N}_2 = -2\Omega^2 \mathrm{Im}D(\omega)$, where $D(\omega)$ is the Fourier trans-

form of the retarded spin-flip correlation function $D(t-t') = -i\theta(t-t')\langle[\sum_{\mathbf{k}} a_{\mathbf{k}1}^{\dagger}(t)a_{\mathbf{k}2}(t), \sum_{\mathbf{k}'} a_{\mathbf{k}'2}^{\dagger}(t')a_{\mathbf{k}'1}(t')]\rangle$. Since the BEC of $|1\rangle$ atoms is weakly interacting, i.e., $n_0 a_{\mathrm{B}}^3 \ll 1$, it can be described up to leading order in $n_0 a_{\mathrm{B}}^3$, yielding $D(\omega) = n_0 G_2(\mathbf{k} = \mathbf{0}, \omega)$ for a homogenous system, where $G_2(\mathbf{k}, \omega)$ is the Green's function for an atom in spin-state $|2\rangle$ with momentum $\mathbf{k}$ and energy ω. It follows that an ideal RF measurement directly probes the $\mathbf{k} = \mathbf{0}$ part of the impurity spectral function, defined as $A(\omega) = -2\mathrm{Im}G_2(\mathbf{k} = \mathbf{0}, \omega)$. Note that we neglect vertex corrections to $D(\omega)$, which are small for $n_0 a_{\mathrm{B}}^3 \ll 1$ as long as the temperature is much smaller than the critical temperature [30]. See Supplementary Information for details on the evaluation of the spectral response, including Fourier broadening and trap averaging.

SUPPLEMENTARY INFORMATION: OBSERVATION OF ATTRACTIVE AND REPULSIVE POLARONS IN A BOSE-EINSTEIN CONDENSATE

I. EXPERIMENTAL DETAILS

A. Feshbach resonance structure

The relevant interactions in our system are determined by two s-wave scattering lengths. The internal interaction of the BEC, which provides the bosonic medium, is governed by the scattering length a_{B}. The properties of the polaron are determined by the interaction between the impurity and the bosonic medium which is governed by the scattering length a.

The experiments are performed with a ^{39}K BEC in the $|1\rangle \equiv |F = 1, m_F = -1\rangle$ state and impurities in the $|2\rangle \equiv |F = 1, m_F = 0\rangle$ state. Three Feshbach resonances contribute to the two relevant scattering lengths as shown in Fig. 5. The background scattering length of ^{39}K is negative, but Feshbach resonances at $33.6\,\mathrm{G}$ and $162\,\mathrm{G}$ create a wide window of positive scattering length which allows stable BEC formation [29, 31]. Within this window, an interstate Feshbach resonance allows us to tune the interactions between the impurity and the medium [25]. In the region where measurements are performed, the scattering length of the medium a_{B} is approximately constant at $9a_0$. The scattering length which characterizes the interaction between atoms in the $|2\rangle$ state is approximately $-20a_0$ in this region.
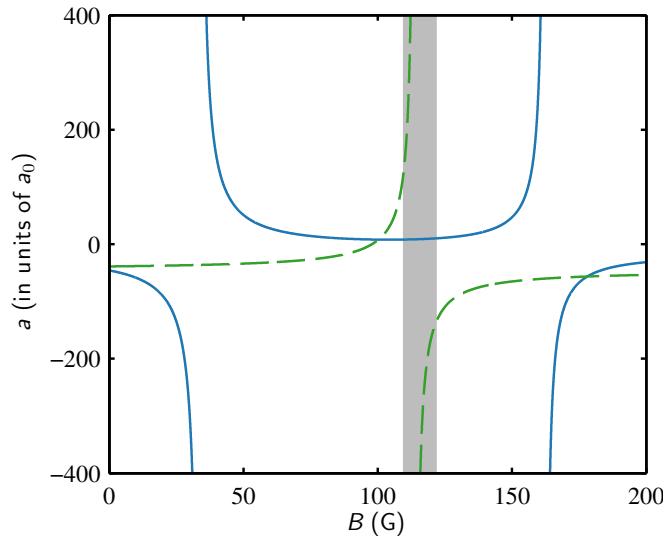

FIG. 5. Feshbach resonance structure of the relevant states in ^{39}K. The solid blue line shows the scattering length of atoms in the $|1\rangle$ state and the dashed green line shows the scattering length between atoms in the states $|1\rangle$ and $|2\rangle$. The shaded gray area displays the region in which measurements are performed.
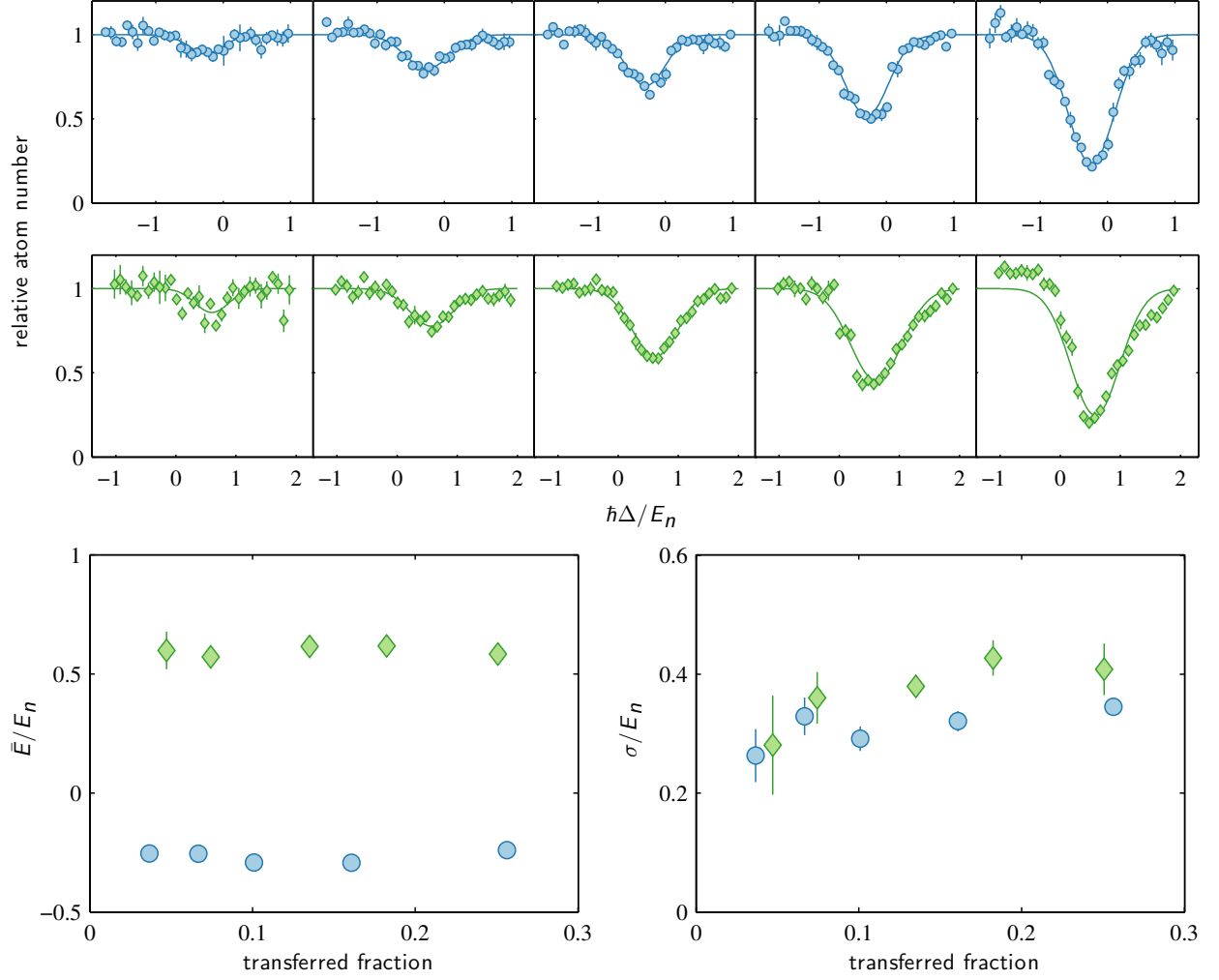
FIG. 6. Polaron signal at various transferred fractions. Remaining number of atoms in the $|1\rangle$ state for $1/k_n a = -0.84$ (top row) and $1/k_n a = 1.6$ (middle row) as a function of the detuning for various RF powers. Bottom: Average energy $\bar{E}$ and width σ of the spectroscopic signal as a function of transferred fraction for $1/k_n a = -0.84$ (circles) and $1/k_n a = 1.6$ (diamonds). The transferred fraction corresponds to a third of the relative loss due to three-body recombination.

B. Polaron fraction

Polarons are formed by applying a RF pulse close to the transition between the $|1\rangle$ and $|2\rangle$ states. A fraction of $|1\rangle$ atoms is transferred to the $|2\rangle$ state and, due to the interaction, polarons are formed (see Sec. II). This method breaks down for large transferred fractions of atoms, since atoms in the $|2\rangle$ state cannot be treated as impurities in this case, and the bosonic medium of $|1\rangle$ atoms is depleted, thus changing its properties.

To investigate possible consequences of these effects, the spectroscopic signal was recorded for various transferred fractions at two values of the interaction parameter $1/k_n a = -0.84$ and $1/k_n a = 1.6$. To vary the transferred fraction, the power of the RF pulse was changed, while keeping the pulse duration constant. The observed signal as well as the resulting average energy and width are shown in Fig. 6.

No significant deviations of the average energy and only a minor increase in width are observed as a function of the transferred fraction. For transferred fractions beyond 15%, a small distortion of the line shape is observed. We attribute this to a combination of BEC depletion, power broadening effects and a non-linear response of the broad many-body continuum part of the spectrum.

Since these effects only appear at transferred fractions well above 10%, it confirms that our measurements are performed within the linear response regime and represent a valid characterization of the polaron.

II. THEORETICAL DESCRIPTION

In this section, we describe the theoretical framework used to interpret the experimental results. We consider the case of an impurity in a uniform BEC with density $n_0 = 2.3 \times 10^{14} \, \text{cm}^{-3}$ at zero temperature. In the next section, we include the trap inhomogeneity using the local density approximation. We take $a_B = 9a_0$ in all theory calculations, such that $k_n a_B \approx 0.01$ and the BEC is weakly interacting. In the following, we set $\hbar$ and the volume to 1.

A. Model of the Feshbach resonance in a ^{39}K BEC

We model the interactions between the $|2\rangle$ impurity atoms and a BEC of $|1\rangle$ atoms using a two-channel Hamiltonian for the Feshbach resonance. Within Bogoliubov mean-field theory for the condensed atoms, we have:

$$\hat{H} = \sum_{\mathbf{k}} \left[E_{\mathbf{k}} \beta_{\mathbf{k}}^\dagger \beta_{\mathbf{k}} + \varepsilon_{\mathbf{k}} a_{\mathbf{k},2}^\dagger a_{\mathbf{k},2} + \left(\varepsilon_{\mathbf{k}}^{\text{d}} + \nu_0 \right) d_{\mathbf{k}}^\dagger d_{\mathbf{k}} \right]$$
$$+ g\sqrt{n_0} \sum_{\mathbf{k}} \left(d_{\mathbf{k}}^\dagger a_{\mathbf{k},2} + h.c. \right) + g \sum_{\mathbf{k},\mathbf{q}} \left(d_{\mathbf{q}}^\dagger a_{\mathbf{q}-\mathbf{k},2} a_{\mathbf{k},1} + h.c. \right). \tag{1}$$

Here, $a_{\mathbf{k}\sigma}$ removes a ^{39}K atom in spin state $|\sigma\rangle$ with momentum $\mathbf{k}$ and single-particle energy $\varepsilon_{\mathbf{k}} = k^2/2m$; m is the mass of the atom, $E_{\mathbf{k}} = \sqrt{\varepsilon_{\mathbf{k}}(\varepsilon_{\mathbf{k}} + 2\mu)}$ is the Bogoliubov dispersion, and $\mu = 4\pi a_B n_0/m$ is the chemical potential of the BEC, where a_B is the scattering length between the $|1\rangle$ atoms. The annihilation operator of $|1\rangle$ atoms is related to the creation and annihilation operators of Bogoliubov modes, $\beta_{\mathbf{k}}^\dagger$ and $\beta_{\mathbf{k}}$ respectively, through $a_{\mathbf{k},1} = u_{\mathbf{k}}\beta_{\mathbf{k}} - v_{\mathbf{k}}\beta_{-\mathbf{k}}^\dagger$. The coherence factors, given by $u_{\mathbf{k}}^2 = [1 + (\varepsilon_{\mathbf{k}} + \mu)/E_{\mathbf{k}}]/2$ and $v_{\mathbf{k}}^2 = [-1 + (\varepsilon_{\mathbf{k}} + \mu)/E_{\mathbf{k}}]/2$, are real and positive. The atoms in the two spin states interact via a closed channel molecule. This has creation operator operator $d_{\mathbf{k}}^\dagger$ at momentum $\mathbf{k}$, single particle energy $\varepsilon_{\mathbf{k}}^{\text{d}} = \varepsilon_{\mathbf{k}}/2$, and a detuning ν_0 from the two-atom $|1\rangle$-$|2\rangle$ threshold. The strength of the interaction is denoted g, and it is taken to be constant for momenta $|\mathbf{k}| < \Lambda$ and is set to 0 above the momentum cutoff Λ. Renormalization of the $|1\rangle$-$|2\rangle$ two-body interaction then yields, respectively, the scattering length and range parameter [32]:

$$a = \frac{mg^2}{4\pi} \frac{1}{\frac{mg^2\Lambda}{2\pi^2} - \nu_0}, \qquad R^* = \frac{4\pi}{m^2g^2}. \tag{2}$$

The range parameter R^* is necessary to fix the size of the smallest (i.e., ground-state) Efimov trimer consisting of two $|1\rangle$ atoms and one $|2\rangle$ atom. Note that previous experimental studies of identical bosons have found that the size of the ground-state Efimov trimer is universally related to the van der Waals range [33], an effect which was explained in Ref. [34]. Hence, it is natural to fix the Efimov physics using two-body parameters. From an investigation of the vacuum three-body problem within the two-channel model, we find that the scattering length at which the ground-state Efimov trimer crosses the three-atom continuum threshold is $a_- \simeq -5000R^*$ [23]. Since $R^* = 60a_0$ in our experiment, we find that $|a_-| = 3 \times 10^5 a_0$, which exceeds the average interparticle spacing by two orders of magnitude. Thus, we expect Efimov physics to play a very small role in the experimental results. We emphasise that this conclusion is independent of the specific manner in which we include Efimov physics; indeed, calculations using realistic interatomic potentials find a similarly large separation of scales between the van der Waals range and a_- [35].

Note that we do not apply the commonly used Fröhlich approximation to the Hamiltonian for the impurity problem, as this would not allow us to consider near resonant interactions. Indeed, the Fröhlich model already misses terms at the third order of perturbation theory [22]. These are on the other hand correctly captured within the variational approach described in Ref. [23], which forms the basis of our evaluation of the entire impurity spectral function.

B. Truncated basis method for the Bose polaron

To approximately model the Bose polaron across the full range of impurity-boson interactions, we apply a truncated basis method (TBM), first introduced in Ref. [27]. This method was successfully used to model both the dynamics and the spectral response for an impurity strongly interacting with a Fermi gas [27], and here we extend the TBM to obtain the spectral function of the Bose polaron.

The TBM consists in truncating the Hilbert space of wavefunctions for the impurity in the BEC. In the present work, we restrict the Hilbert space to wavefunctions containing the impurity, the BEC, and up to 2 Bogoliubov excitations of the BEC. As we shall see, this allows us to capture the attractive and repulsive polaron peaks in the spectral function, as well as the continuum of states in between. Variational wavefunctions with up to one [19] or two [23] Bogoliubov excitations have already

been successfully used to determine the ground-state energy of the Bose polaron; here we extend the use of the variational wavefunction in Ref. [23] to evaluate the entire spectral function of the impurity.

We start by considering an exact energy eigenstate of the system which satisfies the equation:

$$\hat{H}|\psi\rangle = E|\psi\rangle \tag{3}$$

where E is the energy of the state $|\psi\rangle$. We then take truncated wavefunctions of the form: $|\psi\rangle = \sum_j \alpha_j|j\rangle$, where $\{|j\rangle\}$ represents a subset of a complete orthonormal set of states. Inserting this into Eq. (3) and taking the projection with respect to $|j\rangle$ then yields

$$E\alpha_j = \sum_l \langle j|\hat{H}|l\rangle \alpha_l \equiv \sum_l H_{jl}\alpha_l. \tag{4}$$

Diagonalising the Hamiltonian within this subspace then corresponds to determining the eigenvalues and eigenvectors of the matrix H_{jl}.

To determine the spectral function using the TBM, we exploit the relation between the Green's function in time and frequency space:

$$A(\omega) = 2\mathrm{Re}\int_0^\infty dt\, e^{i\omega t}\langle\psi_0|e^{-i\hat{H}t}|\psi_0\rangle = 2\pi\sum_j|\langle\psi_0|\phi_j\rangle|^2 \underbrace{\int_{-\infty}^\infty \frac{dt}{2\pi}e^{i\omega t}e^{-iE_jt}}_{\delta(\omega-E_j)}, \tag{5}$$

where $|\psi_0\rangle$ is the polaron state in the absence of interactions. Here, ϕ_j are the eigenstates of the truncated Hamiltonian, with energies E_j. In practice, the RF pulse is of finite duration in experiment, thus giving rise to a broadening of the measured spectrum. We model this non-zero Fourier width of the RF probe by convolving the spectral function with a Gaussian:

$$I_0(\omega) \equiv \int \frac{d\omega'}{2\pi}A(\omega-\omega')\frac{1}{\sqrt{2\pi}\sigma_{\mathrm{rf}}}e^{-\omega'^2/2\sigma_{\mathrm{rf}}^2} \tag{6}$$

where σ_{rf} corresponds to the Fourier width. Using (6) in (5) yields

$$I_0(\omega) = \sum_j|\langle\psi_0|\phi_j\rangle|^2 \frac{1}{\sqrt{2\pi}\sigma_{\mathrm{rf}}}e^{-(\omega-E_j)^2/2\sigma_{\mathrm{rf}}^2}. \tag{7}$$

For the specific case of an impurity in a BEC, we evaluate the spectrum using wavefunctions of the form

$$|\psi\rangle = \left(\alpha_0 a_{\mathbf{0},2}^\dagger + \sum_{\mathbf{k}}\alpha_{\mathbf{k}}a_{-\mathbf{k},2}^\dagger\beta_{\mathbf{k}}^\dagger + \frac{1}{2}\sum_{\mathbf{k}_1\mathbf{k}_2}\alpha_{\mathbf{k}_1\mathbf{k}_2}a_{-\mathbf{k}_1-\mathbf{k}_2,2}^\dagger\beta_{\mathbf{k}_1}^\dagger\beta_{\mathbf{k}_2}^\dagger + \gamma_0 d_{\mathbf{0}}^\dagger + \sum_{\mathbf{k}}\gamma_{\mathbf{k}}d_{-\mathbf{k}}^\dagger\beta_{\mathbf{k}}^\dagger\right)|\Phi\rangle, \tag{8}$$

with $|\Phi\rangle$ the wavefunction of the weakly interacting BEC. Such a wavefunction was first introduced in Ref. [23], and provided the first many-body theory that included Efimov physics in a BEC. In this work, we include three-body correlations non-perturbatively in the impurity spectral function for the first time.

C. Weak-coupling perturbation theory

In the weak coupling limit, the polaron properties can be calculated perturbatively [22]. Assuming $|a| \ll |a_-|$, the small parameter in this perturbative expansion is a/ξ, where we have defined the BEC coherence length $\xi \equiv 1/\sqrt{8\pi n_0 a_B}$. To third order in a, the quasiparticle energy was calculated in Ref. [22] to be

$$\frac{E}{E_n} = \frac{4}{3\pi}k_n a\left[1 + \frac{8\sqrt{2}}{3\pi}\sqrt{\frac{4k_n a_B}{3\pi}}k_n a + \left(\frac{2}{3} - \frac{\sqrt{3}}{\pi}\right)\frac{4k_n a_B}{3\pi}(k_n a)^2\ln\left(\sqrt{\frac{4k_n a_B}{3\pi}}k_n a\right)\right]. \tag{9}$$

When comparing perturbation theory for the polaron energy with the experimental data in Fig. 3 in the main manuscript, we plot (9) using a k_n obtained from the trap averaged density. In principle, we should average (9) over the cloud, but the difference between the results of the two averaging procedures is negligible in the perturbative regime.

Likewise, the quasiparticle residue of the polaron to third order in a/ξ [22] is

$$Z^{-1} = 1 + \frac{2\sqrt{2}}{3\pi}\frac{2}{\sqrt{3\pi k_n a_B}}(k_n a)^2 + 0.64 \times \frac{4}{3\pi}(k_n a)^3. \tag{10}$$
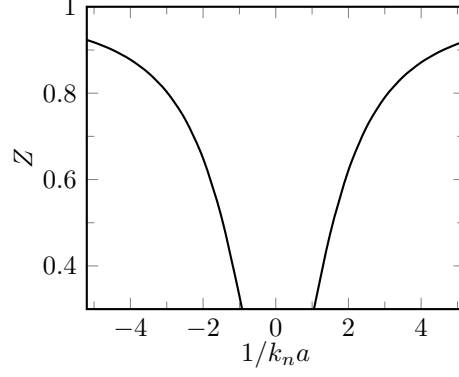
FIG. 7. Quasiparticle residue of the attractive and repulsive polarons in a uniform BEC calculated from the perturbative expression Eq. (10).

Equations (9)-(10) together determine the quasiparticle part of the impurity spectral function, $2\pi Z\delta(\omega - E)$, in the perturbative regime. The quasiparticle peak is dominant when $1 - Z \ll 1$, and it follows from Eq. (10) that this condition corresponds to requiring $(k_n a)^2/\sqrt{k_n a_B} \ll 1$. Since our experimental value $k_n a_B \simeq 0.01$ is very small, this condition is, in fact, stricter than the condition $a/\xi \ll 1$. This means that the quasiparticle residue becomes significantly smaller than one, even when a/ξ is still small. Indeed, we see from Fig. 7, that $Z \geq 2/3$ only for $1/k_n a < -1.8$ or $1/k_n a > 2$.

In addition to the quasiparticle peak, the perturbative calculation can also provide some insight into the broad many-body continuum part of the spectral function. By expanding the self energy of the impurity up to second order in a, we obtain

$$A(\omega) = 2\pi Z\delta(\omega - E) + \theta(\omega)\frac{2}{E_n}\frac{\frac{2\sqrt{2}(k_n a)^2}{3\pi}\frac{[\omega/E_n]^3}{(4k_n a_B/3\pi + \omega/E_n)^{5/2}}}{\frac{\omega^2}{E_n^2} + \left(\frac{2\sqrt{2}(k_n a)^2}{3\pi}\frac{[\omega/E_n]^3}{(4k_n a_B/3\pi + \omega/E_n)^{5/2}}\right)^2}, \tag{11}$$

where $\theta(x)$ is the Heaviside step function, and E is the polaron energy in Eq. (9) up to second order. This result illustrates the typical shape of the impurity spectral function consisting of a quasiparticle peak and a many-body continuum. It furthermore provides a simple physical interpretation of the continuum above the polaron energy for weak interactions: It consists of states formed by a Bogoliubov mode and the impurity moving with opposite momenta. The energy threshold of this continuum is zero within second order perturbation theory, because this is the minimum cost to create an impurity particle with momentum $\mathbf{q}$ and energy $q^2/2m$ plus a Bogoliubov mode with momentum $-\mathbf{q}$ and energy $E_\mathbf{q}$. However, on physical grounds, this continuum of states necessarily starts instead at the polaron energy, since Bogoliubov modes can be excited with arbitrarily small energy and momentum. For large energy $\omega \gg 4\pi a_B n_0/m$, the Bogoliubov modes become ideal gas excitations with energy $\sim q^2/2m$, and the weight of the continuum spectrum of $A(\omega)$ decreases as $\omega^{-3/2}$.

D. Comparison of spectral functions for the uniform system

In Fig. 8, we plot the spectral function, convoluted with a small Fourier width according to (6), in the weak coupling regime $1/k_n a = \pm 5$. We have used three different calculations to obtain $A(\omega)$: perturbation theory given by (11), the truncated basis method with only one Bogoliubov excitation included (TBM1), i.e., neglecting the third and fifth terms in Eq. (8), and the full calculation including two Bogoliubov excitations (TBM2). First, we see that all three calculations agree very well concerning the peak position, which corresponds to the energy of the polaron quasiparticle. This shows that the TBM recovers the perturbative result in the weak-coupling limit, as desired.

For the attractive case, we also see that both the perturbative calculation and TBM1 predict essentially the same many-body continuum, which starts at zero energy as discussed above. TBM2, on the other hand, correctly predicts the continuum to start above the polaron peak (the transition from the polaron peak to the continuum is smoothened due to the small Fourier broadening). This is because the wavefunctions with an extra Bogoliubov mode can describe dressed impurities at finite momentum.

In Fig. 9, we plot the Fourier broadened spectral function for $k_n a = -1$ obtained again from the three different calculations. For this fairly strong coupling, there is poor agreement between perturbation theory and the TBM, as expected. The three calculations give different predictions for the polaron energy as well as for the many-body continuum. In this regime, perturbation theory is not accurate and the TBM with two Bogoliubov modes is the most reliable, since it includes up to 3-body correlations non-perturbatively.
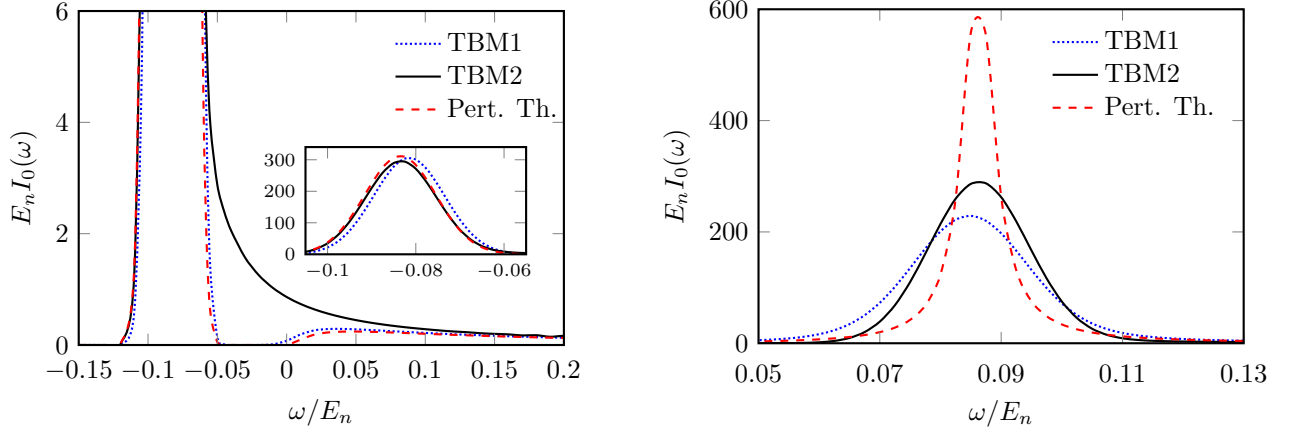
FIG. 8. Spectral function for the impurity in a uniform BEC with $1/k_n a = -5$ (left) and $1/k_n a = 5$ (right) including a small Gaussian broadening $\sigma_{\rm rf}/E_n = 0.008$. The dashed line is the result of perturbation theory, the dotted line the TBM including only one Bogoliubov excitation, and the solid line the TBM including two Bogoliubov excitations. The inset shows the polaron peak for $1/k_n a = -5$.
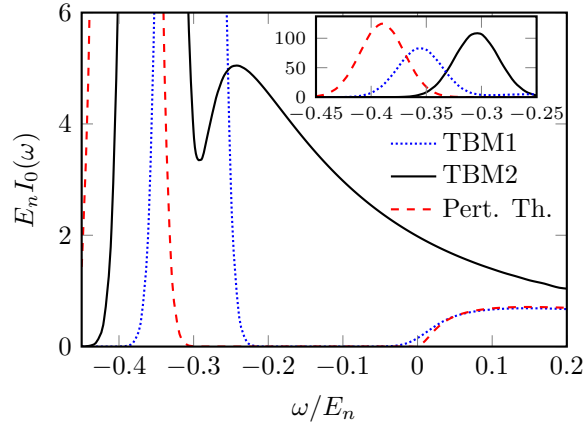

FIG. 9. Calculated spectral function for the impurity in a uniform BEC with $1/k_n a = -1$ and a small Gaussian broadening $\sigma_{\rm rf}/E_n = 0.020$. Lines and inset are as in Fig. 8.

III. TRAP AVERAGED SPECTRA

The preceding analysis was for an impurity in a BEC of uniform density n_0. However, in the experiment, the atomic BEC is confined in a harmonic trap, and instead has *average* density n_0, with corresponding k_n. On the scale of the trap, the RF probe is essentially uniform, transferring atoms from the $|1\rangle$ state into the $|2\rangle$ state in all regions of the inhomogeneous BEC. This in turn gives rise to a broadening of the observed spectral response of the impurity atom, since it is surrounded by a BEC of varying density $n(\mathbf{r})$. We take this into account using the local density approximation to average the response over the cloud:

$$I(\omega) = \frac{1}{N} \int d^3\mathbf{r}\, n(\mathbf{r}) I_0(\omega, n(\mathbf{r})). \tag{12}$$

Here $I_0(\omega, n(\mathbf{r}))$ is the local Fourier broadened response obtained from (6) using an impurity spectral function $A(\omega)$ corresponding to the density $n(\mathbf{r}) = \frac{m}{4\pi\hbar^2 a_{bb}}\mu(\mathbf{r})$ with $\mu(\mathbf{r}) = \mu - V_{\rm trap}(\mathbf{r})$.

For weak interactions, the spectral function is dominated by the quasiparticle peak, such that Eq. (12) becomes

$$I(\omega) \simeq \frac{1}{N} \int d^3 r\, n(r) \frac{1}{\sqrt{2\pi\sigma_{\rm rf}^2}} e^{\frac{(\omega - E(r))^2}{2\sigma_{\rm rf}^2}}. \tag{13}$$

where $E(\mathbf{r})$ is the local quasiparticle energy at position $\mathbf{r}$ in the trap. This is the expression used to calculate the perturbative spectral width in Fig. 4 of the main manuscript. In the limit $|k_n a| \ll 1$, the width of the spectral signal is dominated by the Fourier
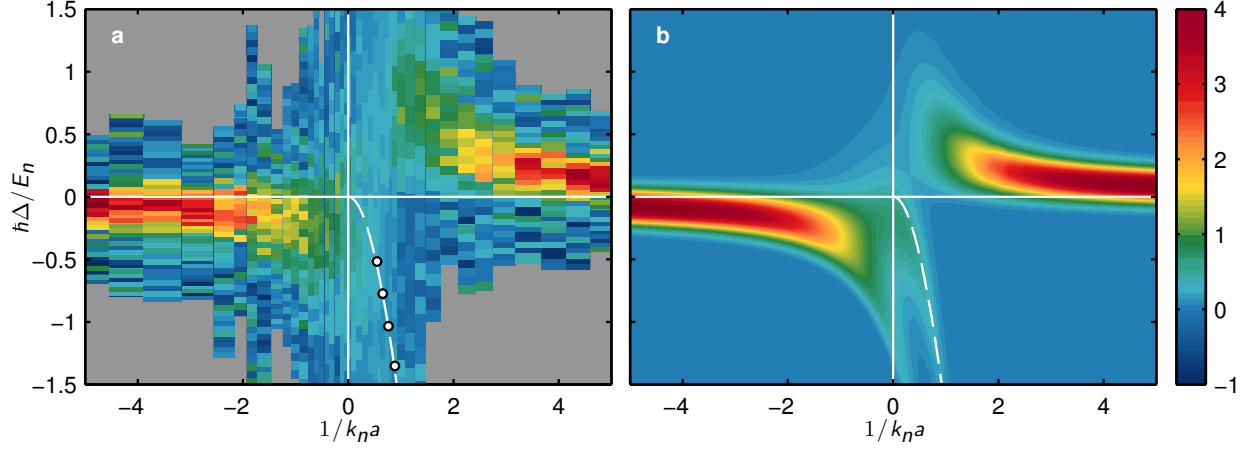
FIG. 10. The experimental spectrum (a) and the trap-averaged spectral function calculated within TBM (b), both normalised so that the frequency integrated weight is the same for each interaction strength. The experimental Fourier width is estimated to be $\sigma_{\rm rf} \simeq 0.08 E_n$.

width $\sigma_{\rm rf}$ of the RF probe, since the trap averaging only occurs over a small range of local interaction parameters. However, for stronger coupling, the signal is averaged over an increasingly larger range of local interaction parameters and thus the trap inhomogeneity can significantly broaden the quasiparticle peak. In this regime, the many-body continuum is also modified by the trap.

The full trap-averaged spectral function obtained within TBM is shown in Fig. 10 together with the experimental result. The exact same data is presented in Fig. 2 of the main text, but here we normalise so that the frequency integrated weight is the same for each interaction strength. This illustrates more clearly how the spectral weight of the many-body continuum suppresses that of the quasiparticle peak in the strongly interacting unitary region.

[1] Schirotzek, A., Wu, C.-H., Sommer, A. & Zwierlein, M. W. Observation of Fermi polarons in a tunable Fermi liquid of ultracold atoms. *Phys. Rev. Lett.* **102**, 230402 (2009).

[2] Kohstall, C. *et al.* Metastability and coherence of repulsive polarons in a strongly interacting Fermi mixture. *Nature* **485**, 615–618 (2012).

[3] Koschorreck, M. *et al.* Attractive and repulsive Fermi polarons in two dimensions. *Nature (London)* **485**, 619–622 (2012).

[4] Landau, L. D. & Pekar, S. I. Effective mass of a polaron. *Zh. Eksp. Teor. Fiz.* **18**, 419 (1948).

[5] Mahan, G. *Many-Particle Physics* (Kluwer Academic/Plenum Publishers, 2000).

[6] Gershenson, M. E., Podzorov, V. & Morpurgo, A. F. *Colloquium* : Electronic transport in single-crystal organic transistors. *Rev. Mod. Phys.* **78**, 973–989 (2006).

[7] Baym, G. & Pethick, C. *Landau Fermi-Liquid Theory: Concepts and Applications* (Wiley-VCH, 1991).

[8] Dagotto, E. Correlated electrons in high-temperature superconductors. *Rev. Mod. Phys.* **66**, 763–840 (1994).

[9] Spethmann, N. *et al.* Dynamics of single neutral impurity atoms immersed in an ultracold gas. *Phys. Rev. Lett.* **109**, 235301 (2012).

[10] Zipkes, C., Palzer, S., Sias, C. & Kohl, M. A trapped single ion inside a Bose-Einstein condensate. *Nature* **464**, 388–391 (2010).

[11] Schmid, S., Härter, A. & Denschlag, J. H. Dynamics of a cold trapped ion in a Bose-Einstein condensate. *Phys. Rev. Lett.* **105**, 133202 (2010).

[12] Balewski, J. B. *et al.* Coupling a single electron to a Bose-Einstein condensate. *Nature* **502**, 664–667 (2013).

[13] Scelle, R., Rentrop, T., Trautmann, A., Schuster, T. & Oberthaler, M. K. Motional coherence of fermions immersed in a Bose gas. *Phys. Rev. Lett.* **111**, 070401 (2013).

[14] Ospelkaus, S. *et al.* Localization of bosonic atoms by fermionic impurities in a three-dimensional optical lattice. *Phys. Rev. Lett.* **96**, 180403 (2006).

[15] Cucchietti, F. M. & Timmermans, E. Strong-coupling polarons in dilute gas Bose-Einstein condensates. *Phys. Rev. Lett.* **96**, 210401 (2006).

[16] Huang, B.-B. & Wan, S.-L. Polaron in Bose-Einstein-condensation system. *Chinese Physics Letters* **26**, 080302 (2009).

[17] Tempere, J. *et al.* Feynman path-integral treatment of the BEC-impurity polaron. *Phys. Rev. B* **80**, 184504 (2009).

[18] Rath, S. P. & Schmidt, R. Field-theoretical study of the Bose polaron. *Phys. Rev. A* **88**, 053632 (2013).

[19] Li, W. & Das Sarma, S. Variational study of polarons in Bose-Einstein condensates. *Phys. Rev. A* **90**, 013618 (2014).

[20] Grusdt, F., Shchadilova, Y. E., Rubtsov, A. N. & Demler, E. Renormalization group approach to the Fröhlich polaron model: application to impurity-bec problem. *Scientific Reports* **5**, 12124 (2015).

[21] Ardila, L. A. P. & Giorgini, S. Impurity in a Bose-Einstein condensate: Study of the attractive and repulsive branch using quantum Monte Carlo methods. *Phys. Rev. A* **92**, 033612 (2015).

[22] Christensen, R. S., Levinsen, J. & Bruun, G. M. Quasiparticle properties of a mobile impurity in a Bose-Einstein condensate. *Phys. Rev. Lett.* **115**, 160401 (2015).

[23] Levinsen, J., Parish, M. M. & Bruun, G. M. Impurity in a Bose-Einstein condensate and the Efimov effect. *Phys. Rev. Lett.* **115**, 125302 (2015).

[24] Zwierlein, M. W., Hadzibabic, Z., Gupta, S. & Ketterle, W. Spectroscopic insensitivity to cold collisions in a two-state mixture of fermions. *Phys. Rev. Lett.* **91**, 250404 (2003).

[25] Lysebo, M. & Veseth, L. Feshbach resonances and transition rates for cold homonuclear collisions between ^{39}K and ^{41}K atoms. *Phys. Rev. A* **81**, 032702 (2010).

[26] Efimov, V. Energy levels arising from resonant two-body forces in a three-body system. *Phys. Lett. B* **33**, 563–564 (1970).

[27] Cetina, M. *et al.* Ultrafast many-body interferometry of impurities coupled to a Fermi sea. To be published.

[28] Makotyn, P., Klauss, C. E., Goldberger, D. L., Cornell, E. A. & Jin, D. S. Universal dynamics of a degenerate unitary Bose gas. *Nat Phys* **10**, 116–119 (2014).

[29] Wacker, L. *et al.* Tunable dual-species Bose-Einstein condensates of ^{39}K and ^{87}Rb. *Phys. Rev. A* **92**, 053602 (2015).

[30] Pethick, C. J. & Stoof, H. T. C. Collisional frequency shifts of absorption lines in an atomic hydrogen gas. *Phys. Rev. A* **64**, 013618 (2001).

[31] D'Errico, C. *et al.* Feshbach resonances in ultracold ^{39}K. *New Journal of Physics* **9**, 223 (2007).

[32] Petrov, D. S. Three-boson problem near a narrow feshbach resonance. *Phys. Rev. Lett.* **93**, 143201 (2004).

[33] Berninger, M. *et al.* Universality of the three-body parameter for Efimov states in ultracold cesium. *Phys. Rev. Lett.* **107**, 120401 (2011).

[34] Wang, J., D'Incao, J. P., Esry, B. D. & Greene, C. H. Origin of the three-body parameter universality in Efimov physics. *Phys. Rev. Lett.* **108**, 263001 (2012).

[35] Wang, Y., Wang, J., D'Incao, J. P. & Greene, C. H. Universal three-body parameter in heteronuclear atomic systems. *Phys. Rev. Lett.* **109**, 243201 (2012).